International Journal of Mass Spectrometry 279 (2009) 41–46

Contents lists available at ScienceDirect

International Journal of Mass Spectrometry

journal homepage: www.elsevier.com/locate/ijms

Au-assisted visible laser MALDI

Lee Chuin Chen[a], Kunihiko Mori[a], Hirokazu Hori[b,*], Kenzo Hiraoka[a,**]

[a] Clean Energy Research Center, University of Yamanashi, 4-3-11 Takeda, Kofu 400-8511, Japan
[b] Interdisciplinary Graduate School of Medical and Engineering, University of Yamanashi, 4-3-11 Takeda, Kofu 400-8511, Japan

ARTICLE INFO

Article history:
Received 4 July 2008
Received in revised form 9 October 2008
Accepted 10 October 2008
Available online 21 October 2008

Keywords:
MALDI
Gold
Nanoparticle
Visible laser
Surface plasmon resonance

ABSTRACT

The excitation of UV-absorbing MALDI matrixes with visible laser (532 nm wavelength) and the desorption/ionization of biomolecules were performed by coating the analytes doped matrix with Au thin film (5–10 nm) using ion sputtering deposition. The Au film was first ablated with the laser of higher fluence, resulting in a crater/hole about the size of the laser beam spot on the target. After a few initial laser shots, analytes and matrix related ions were observed from the crater even at lower laser fluence. Electron microscopy inspection on the laser ablated region revealed the formation of nanoparticles with sizes ranging from <10 to 50 nm. Compared with the infra-red laser (1064 nm) excitation, the visible laser produced much higher abundance of matrix radical ions, and less heating effect as measured by the thermometer molecules. The results suggest the photo-excitation and photo-ionization of matrix molecules by the visible laser, possibly assisted by the gold nanoparticles and nanostructures left on the ablated crater.

1. Introduction

Owing to their fascinating optical and chemical properties, metallic nanoparticles and nanostructures have attracted considerable attention in various research fields. Functionalized or conjugated gold nanoparticles, which have high binding affinity to specific analytes are used for bio-sensing [1], and DNA detection [2]. Selective laser photo-thermal therapy using nanoparticles had also been proposed for cancer treatment [3].

For metallic nanoparticles and nanostructures, their optical responses are governed by the excitation of surface plasmon [4,5], and at the surface plasmon resonance, all the free electrons within the conduction band will oscillate in-phase, leading to optical near-field enhancement at a small volume. The surface plasmon-induced electromagnetic field enhancement on the metallic nanoparticles had been known to be accountable for the surface-enhanced Raman spectroscopy (SERS) [6], and non-linear optical response such as second harmonic generation [7,8], and optical frequency mixing [9]. For the gold nanoparticles with diameter of ≤10–50 nm, the surface plasmon resonates at ~520 nm with wide absorption band, which can be readily excited by a frequency-doubled Nd:YAG laser of 532 nm wavelength.

On the metal surface, the metal-absorbates electronic coupling had also been known to have contributed to the chemical enhancement for SERS [10–12]. Upon absorption on the metal surface, the interaction between the absorbate molecules and the electron gas on the metal surface results in the broadening and shifting in energy of the free molecular states [10]. Thus, even though the states transition of the free molecule may be too energetic to be excited by, say a visible laser, a near resonance could be found for the laser once molecule is adsorbed on the metal surface.

Matrix-assisted laser desorption/ionization (MALDI) mass spectrometry is an effective and soft method in obtaining mass spectra for synthetic and biological samples with less molecular fragmentation [13,14]. The established UV-MALDI method usually employs a nitrogen laser (337 nm, 3.68 eV), or a frequency-tripled Nd:YAG laser (355 nm, 3.49 eV) for desorption/ionization. Although the detailed desorption/ionization mechanism of MALDI had not been thoroughly understood, it is generally believed that the radical ions of the matrix molecules produced by either two photon ionization or the molecular exciton pooling, play crucial roles in ionizing the desorbed analytes [15,16]. Despite efforts by various research groups [17–19], efficient chemical matrix for visible laser has not been found thus far, and the existing matrixes are not accessible by the laser wavelength ranging from 400 nm to ~2.7 μm.

Another technique of UV-MALDI involves the use of inorganic nanoparticles in liquid suspension (two-phase matrix). The use of nanoparticles as efficient UV absorbers was first introduced by Tanaka et al., in which 30 nm cobalt powders were suspended in glycerol solution [13]. Hence, a variety of materials, including gold

* Corresponding author. Tel.: +8155 220 8676.
** Corresponding author. Tel.: +8155 220 8572.
E-mail addresses: hirohori@yamanashi.ac.jp (H. Hori), hiraoka@yamanashi.ac.jp (K. Hiraoka).

1387-3806/$ – see front matter © 2008 Elsevier B.V. All rights reserved.
doi:10.1016/j.ijms.2008.10.005

nanoparticles had also been used successfully as inorganic matrixes [20–22]. Recently, we had also demonstrated visible laser desorption/ionization on gold nanostructures, in which the enhanced optical absorption of the nanostructured substrate was due to the surface plasmon resonance [23,24]. However, the ionization mechanism is not thoroughly known, and it is usually assumed that the heating is the only process induced by the nanoparticles upon photon absorption.

In this work, we demonstrate that the UV-absorbing MALDI matrix could also be excited by the visible laser with the presence of gold nanoparticles. Although metallic nanoparticles are usually prepared by chemical reduction methods [25], relatively pure nanoparticles can also be produced by simple laser ablation of the bulk metal [26,27]. In this study, the MALDI matrix surface was first coated with Au thin film (5–10 nm) and gold nanoparticles were formed and deposited on the matrix by laser ablation of the Au film in vacuum. Coating the bio-sample with Au thin film is common in the secondary ion mass spectrometry (SIMS) [28], and recently, it has also been reported to improve the UV-MALDI imaging [29]. However, it should be noted that in our experiment, the Au thin film on the laser spot will be first ablated, and the Au nanoparticles and/or nanostructure, which were left on the crater were used to excite the matrix molecules using a visible laser.

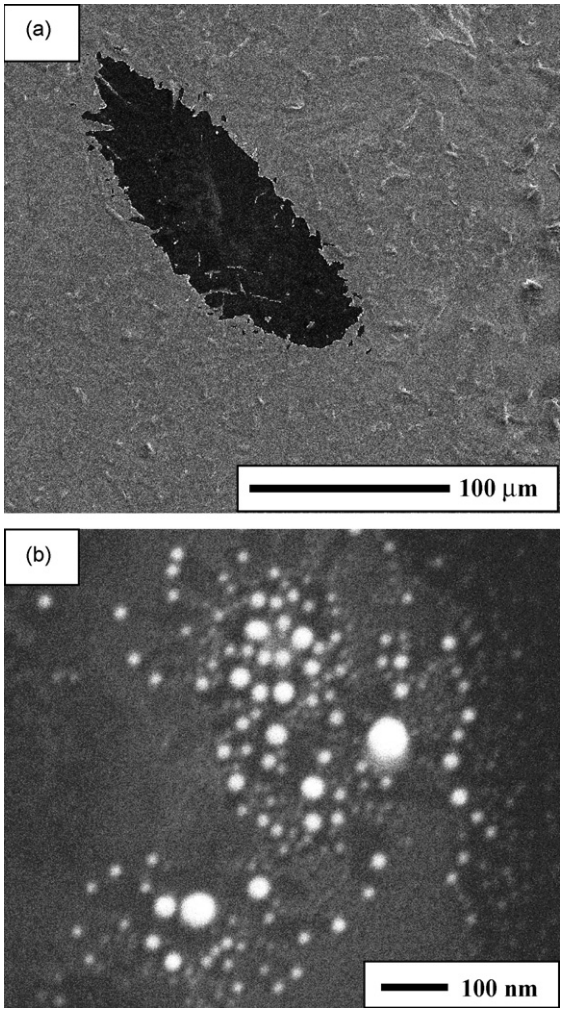

Fig. 1. SEM images showing the ablation of Au by the Nd:YAG laser. (a) The crater formed after the laser ablation of Au thin film. (b) Close-up on the ablated region showing the formation of Au nanoparticles by the laser ablation.

2. Experimental

2.1. Sample preparation

All chemicals and analytes were used as received. The matrix was super-DHB (9:1 mixture of 2,5-dihydroxybenzoic acid, and 2-hydroxy-5-methoxybenzoic acid) obtained from FLUKA. The matrix and bradykinin were dissolved in purified water. For the measurement that involves the desorption/ionization of analytes, the matrix (10–100 mg/ml) were mixed with the analytes (100 μM to 1 mM) at a ratio of 1:1. The matrix or mixture was pipetted onto the stainless steel target plate or silicon substrate and the droplet was gently dried under warm air flow. When the droplet was dried, the analytes doped matrix was coated with a thin layer of gold film (thickness 5–10 nm) using argon ion sputtering coater. After coated, the sample was transferred into the vacuum chamber of the time-of-flight mass spectrometer.

2.2. Synthesis of thermometer molecules

4-Chloro-benzylpyridinium chloride (4CBP) was used as the thermometer molecule and was synthesized according to the lit-

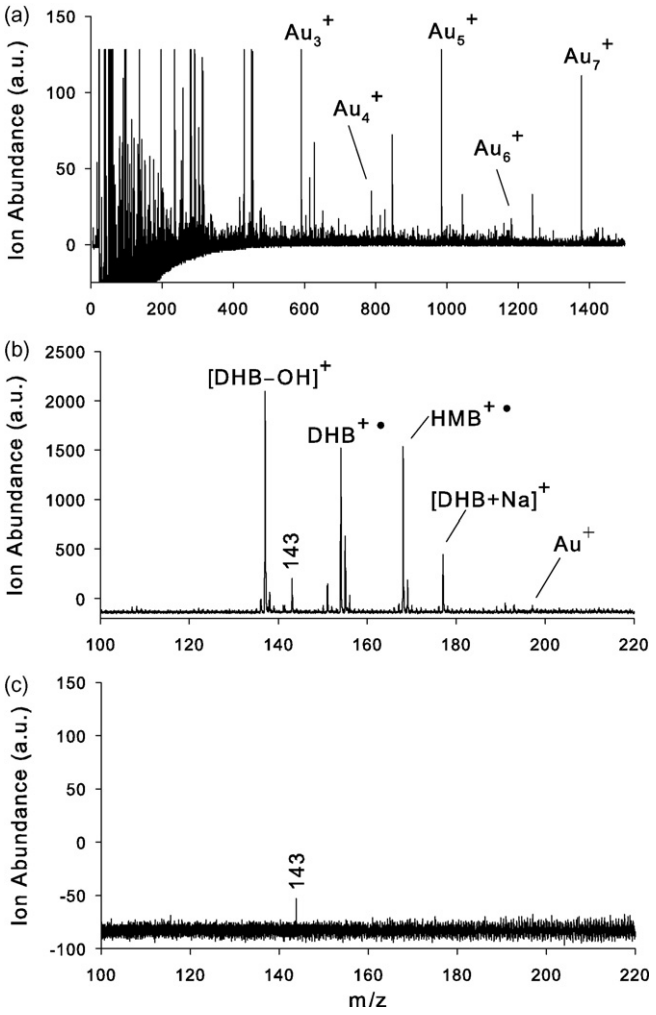

Fig. 2. (a) Mass spectrum of the ablated Au cluster ions at the first ablation laser shot on the Au thin film. (b) Mass spectrum of super-DHB (2,5-dihydroxybenzoic acid, DHB and 2-hydroxy-5-methoxybenzoic acid, HMB) acquired after 10 initial laser shots using 532 nm visible laser. (c) Visible laser desorption/ionization mass spectrum of the super-DHB without Au coating.

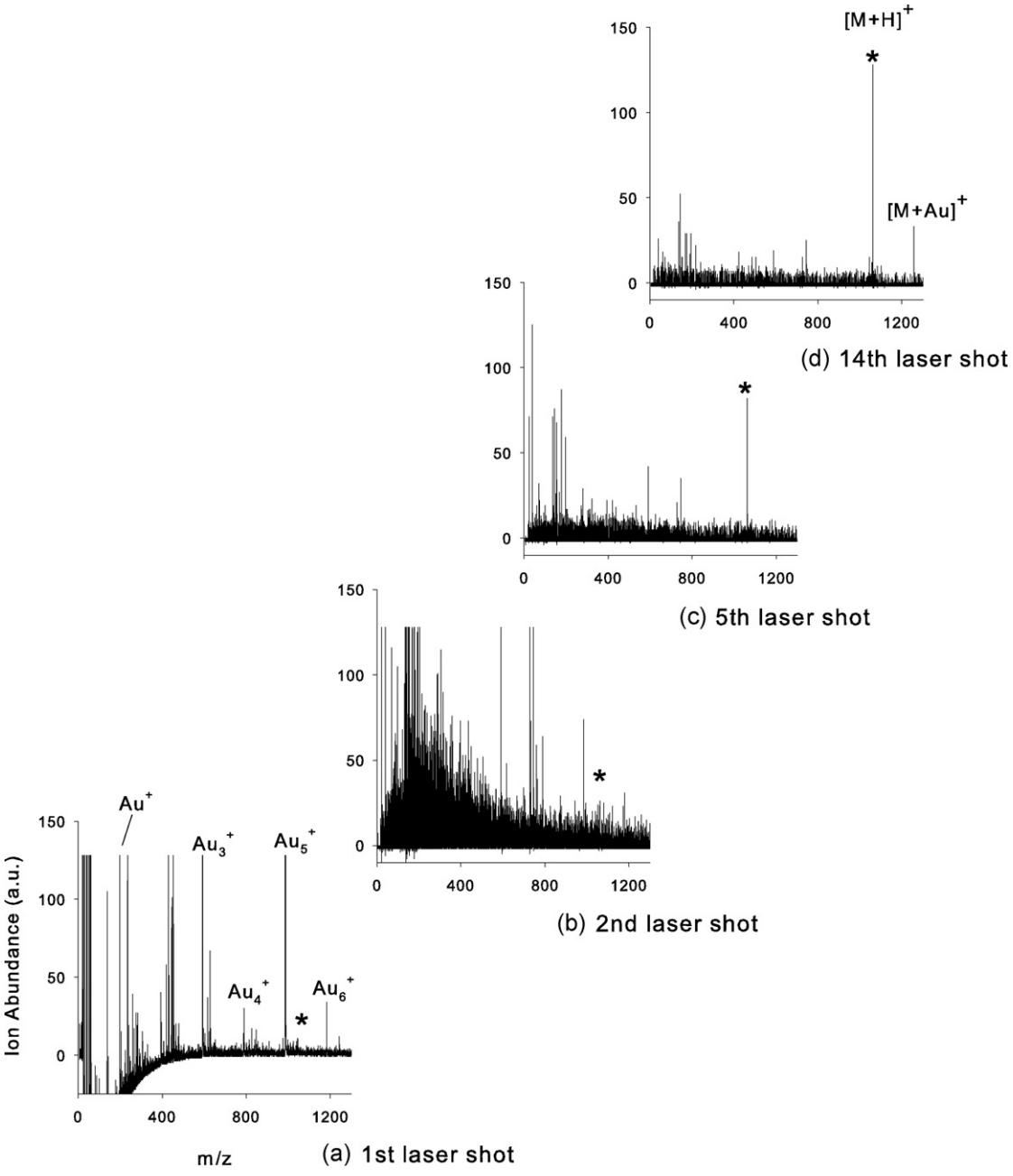

Fig. 3. Single shot visible laser MALDI mass spectra of Au coated bradykinin and matrix mixture obtained at (a) 1st, (b) 2nd, (c) 5th, (d) 14th laser shot. *Denotes the location of $[M+H]^+$.

erature [30]. The pyridine containing benzylchloride was heated at 60 °C for 5∼6 h, and the white solid salts were collected after the pyridine was evaporated. The pyridinium salts were used without further purification.

2.3. Time-of-flight mass spectrometer

The laser desorption/ionization experiment was performed with a 2.5-m time-of-flight mass spectrometer (JMS 2500, JEOL, Japan) with delayed ion extraction. The instrument was operated in reflectron mode. The acceleration voltage for ions was 20 kV and the vacuum pressure in the ion detector was 5×10^{-7} Torr. A linearly polarized frequency-doubled Nd:YAG laser (532 nm wavelength and pulse width of 4 ns) was used for the desorption/ionization experiment. The incident angle of the laser beam was 60° to the surface normal, and the laser polarization was adjusted to be p-polarized using a half-wave plate.

2.4. Laser ablation of Au film

The experiment began by ablating the Au film which was pre-coated on the MALDI matrix. The laser fluence was first adjusted to ablate the bulk Au film, and the generated ions by the ablation were monitored by the mass spectrometer. At this ablation fluence, Au cluster ions were produced in high abundance at the first and second laser shot, and these ions signal decayed rapidly with the subsequent laser shots. The ablation resulted in a crater/hole about the size of the laser beam spot size on the target (∼200 μm). After a few laser shots, the Au ions were significantly reduced, and the laser fluence was slightly reduced to acquire the MALDI mass

spectra. Unless otherwise stated, the mass spectra for matrix and analytes were acquired after 5–10 initial laser shots, and from the accumulation of 30–100 single-shot ion signals. Each mass spectrum in the following section represents the ions produced from a fixed position, that is, from the same crater/hole formed by the laser ablation.

3. Results and discussion

Fig. 1a shows the scanning electron microscope (SEM) image of the Au thin film ablated by the Nd:YAG laser after several laser shots. Since the target was irradiated at ~60° incident angle, the ablated crater was of an elliptical shape with a major axis of ~200 μm. A close-up inspection on the ablated region showed the formation of gold nanoparticles with size ranging from <10 nm to ~50 nm (Fig. 1b). Several processes could be conceivable for the formation of the gold nanoparticles on the sample surface, e.g., the melting of the Au film, and the re-deposition of the ablated Au clusters back onto the surface. Some nanoparticles could also be embedded into the matrix after ablation due to migration. Considerable heating was also expected in the initial ablation laser shots.

The typical first laser shot mass spectrum is shown in Fig. 2a. The first laser shot almost ablated the whole Au film on the laser spot and the mass spectrum was dominated by intense Au cluster ion signals. Because the Au film was deposited on the matrix surface, the laser ablation of Au film has little effect to assist the desorption of the underneath matrix. Fig. 2b shows the mass spectrum of super-DHB (2,5-dihydroxybenzoic acid [DHB, 154 Da] and 2-hydroxy-5-methoxybenzoic acid [HMB, 168 Da]) acquired after 10 initial laser shots. The desorbed ions consist of $DHB^{+\bullet}$, $[DHB+H]^+$, $[DHB+Na]^+$, $[DHB-OH]^+$, $HMB^{+\bullet}$, and $[HMB+H]^+$, which are the typical matrix related ions observed in UV-MALDI. Gold ions Au^+ also appeared in the mass spectrum, but with relatively lower abundance. Irradiating the matrix without Au coating, produced no observable matrix ions (Fig. 2c).

The mass spectra of analytes obtained by the visible laser excited MALDI matrix are shown in Figs. 3 and 4. Fig. 3a–d shows the single shot mass spectra that correspond to the successive laser shots. The mass spectra are dominated by the Au cluster ions during first few laser shots, and no analyte ion is observed (Fig. 3a–b). The *m/z* for $[M+H]^+$ is denoted as * in the mass spectra. The analyte and the matrix related ions became apparent after 5th laser shot and lasted for more than 50 laser shots from a single spot. Since the initial ablation laser shots did not produce any analyte ions except the huge abundance of Au clusters, these "initial ions" will be excluded in the following analysis.

Fig. 4a shows the mass spectrum of the bradykinin (1060 Da) acquired by accumulation of 26 single shot spectra from the same laser spot. Protonated bradykinin ion ($[M+H]^+$) was observed as the base peak with some contribution from metal ion adducts ($[M+Na]^+$ and $[M+Au]^+$). $[DHB+Au]^+$ was, however, not observed.

Comparison was also made with the platinum and silver nanoparticles prepared with the same laser ablation method.

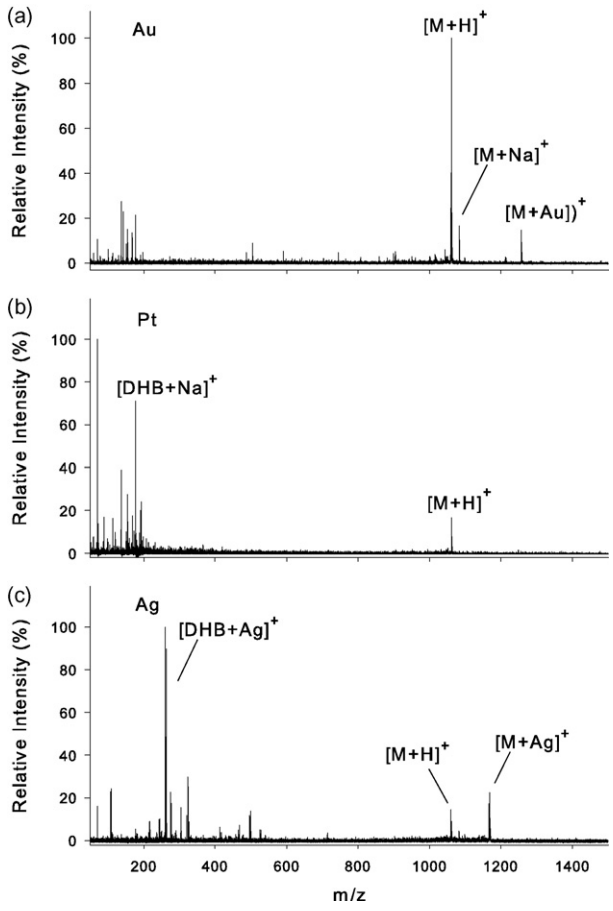

Fig. 4. Visible-MALDI mass spectra of bradykinin assisted by (a) gold, (b) platinum, and (c) silver nanoparticles formed by laser ablation on the metal films. The matrix was super-DHB (9:1 mixture of 2,5-dihydroxybenzoic acid, and 2-hydroxy-5-methoxybenzoic acid).

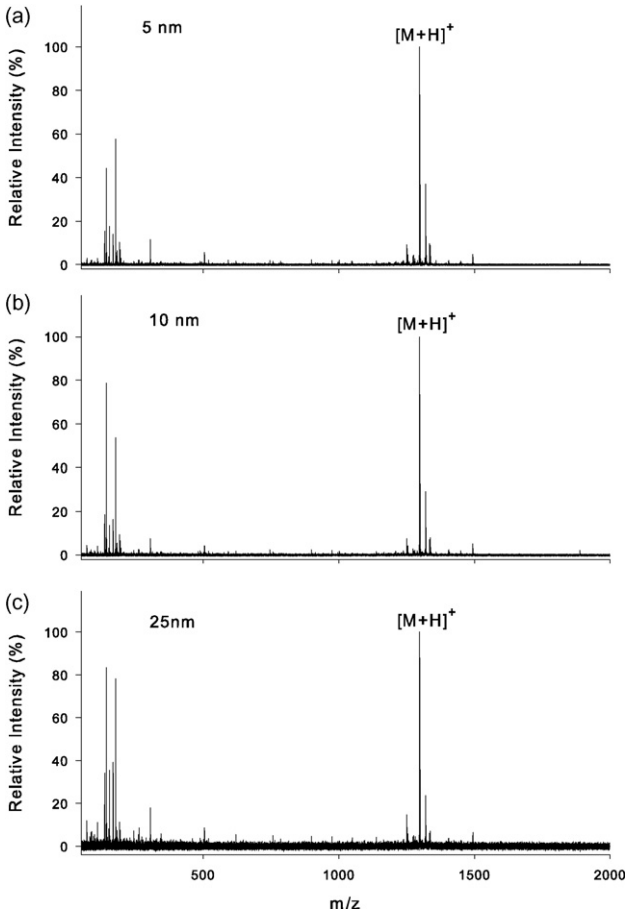

Fig. 5. Visible laser MALDI-MS of angiotensin I assisted by Au nanoparticles formed by laser ablation of (a) 5 nm, (b) 10 nm, and (c) 25 nm Au film. The matrix was super-DHB (9:1 mixture of 2,5-dihydroxybenzoic acid, and 2-hydroxy-5-methoxybenzoic acid).

Visible MALDI mass spectra of bradykinin assisted by platinum and silver nanoparticles are shown, respectively, in Fig. 4b and c. Although analyte ion signal was also observed from platinum nanoparticles, the ion intensity was not as strong (Fig. 4b) as that of Au nanoparticles at the same laser fluence. In the case of silver in Fig. 4c, the mass spectrum was dominated by the silver ion adducts of the matrix, $[DHB+Ag]^+$, and the protonation of analyte was largely suppressed. The abundance of $[M+Ag]^+$ ion appeared to be higher than $[M+H]^+$.

The matrix-assisted visible laser desorption/ionization of angiotensin I from the Au coatings of different initial thickness are shown in Fig. 5. The initial Au film thickness was found to affect the optimization of laser fluence for the film ablation and the generation of analyte ions. The optimum initial thickness was in the range of 5–10 nm (Fig. 5a and b), and for thicker coating (>25 nm), higher laser fluence was needed to produce the equivalent ablation effect as well as for the desorption/ionization of analytes. As shown in Fig. 5c, the ion intensity was also reduced probably due to larger average size of the nanoparticles formed from the thicker Au film.

The thermal property of the Au-assisted visible laser MALDI was examined using 4-chloro-benzylpyridinium chloride (4CBP) as the thermometer molecule. The survival yield of the thermometer molecule, S reflects the internal energy gained from the neighboring matrix molecules either in the solid phase or gas phase [31], and is given as: $S = I(M^+)/[I(M^+) + I(F^+)]$, where $I(M^+)$ and $I(F^+)$ are the abundances of molecular ion (M^+) and the fragment ion (F^+) of 4CBP, respectively. For comparison, the measurement was conducted with three different laser wavelengths (355 nm, 532 nm and 1064 nm) and the thermometer molecule was mixed with the matrix (super-DHB) at a molar ratio of ~1/500. For the case of visible (532 nm) and IR (1064 nm) lasers, the mixture was coated with ~10 nm Au, and after 5–10 laser ablation shots, the laser fluence was slightly reduced to acquire the mass spectra. For UV-MALDI, the same sample (with Au coating) was irradiated with the UV laser (355 nm) at optimum laser fluence, without laser ablation.

The mass spectra and the survival yield of 4CBP acquired using UV, visible and IR lasers are shown in Fig. 6a–c, respectively. The highest survival yield for 4CBP was obtained with UV-MALDI as the UV laser excited the matrix electronically (Fig. 6a, survival yield ~0.9). For the Au nanoparticles assisted MALDI using 532 nm visible laser (Fig. 6b), the survival yield of 4CBP exceeded 0.8 at the typical threshold laser fluence, but is lower than that of the UV irradiation, indicating some heating effect produced by the gold nanoparticles. In Fig. 6c, the mass spectrum was obtained with the IR laser of 1064 nm wavelength which is away from the surface plasmon resonance and is less energetic to induce sufficient electronic excitation. Although the matrix radical ions were also observed, it was of much lower abundance and of poor shot-to-shot repeatability. The low survival yield (~0.65) of 4CBP also indicates considerable heating when the IR laser was used. In sum, the results suggest that the excitation of matrix molecules with the presence of gold nanoparticles is rather wavelength dependent, and the heating effect produced by the nanoparticles, could not solely contribute to the observed ions.

In a separate experiment, we demonstrated that the Au nanoparticles prepared by the laser ablation method was also SERS-active by performing the Raman spectroscopy on Rhodamine 6G. About 0.5 μl of Rhodamine 6G (~1 mM) was deposited on the glass substrate and after dried, the sample was coated with ~10 nm Au using sputtering deposition. The Au-coated Rhodamine 6G was irradiated by one ablation laser shot with 532 nm laser in vacuum. The Raman spectroscopy was conducted using micro-Raman monochromator spectrometer (NRS-2100, Jasco, Japan), and the excitation source was a continuous-wave 488-nm argon laser. The operating laser power was about 3 mW and the exposure time was

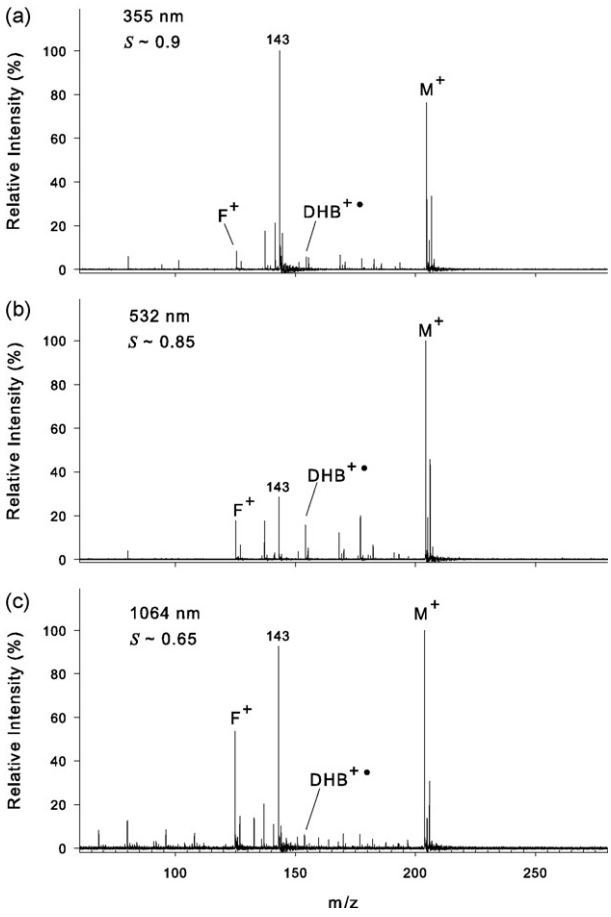

Fig. 6. The MALDI mass spectra of thermometer molecule (4CBP) using (a) 355 nm UV laser, (b) 532 nm visible laser with the presence of Au nanoparticles, and (c) 1064 nm IR laser with the presence of Au nanoparticles. F^+ denotes to the fragment ion of 4CBP. S is survival yield of the thermometer molecule.

10 s. The Raman spectrum of Au coated Rhodamine 6G after laser ablation is shown in Fig. 7a. The prominent peaks are at 1195, 1365, 1539, and 1651 cm^{-1}. Raman spectra obtained from those without laser ablation and without Au coating are shown, respectively, in Fig. 7b and c. Although SERS signal was also observed from the unablated Au coating (Fig. 7b), as the Au film may form nanostructure on the surface rather than a homogeneous layer, the intensity is much weaker compared to that in Fig. 7a where Au nanoparticles were formed by the laser ablation.

Regarding the ionization mechanism for DHB, it is generally believed that in the case of UV excitation (e.g., using nitrogen laser or frequency-tripled Nd:YAG laser), the main processes involve multi-photons photo-ionization, and/or the exciton pooling, in which two or more excited matrix molecules pool their energies to form radical ions [16]. For DHB, the ionization potential (IP) is ~8 eV and the energy for first excited state is 3.466 eV [32]. For the visible laser (532 nm wavelength, 2.33 eV) employed in our experiment, at least three or more photons are needed for multi-photon ionization, and two photons for excitation. Although the presence of Au nanoparticles increases the thermal heating of the matrix molecules, which could lead to the phase evaporation and molecular desorption, it remains questionable if the thermal process is sufficient for the excitation and ionization of the matrix molecules.

As the gold nanoparticles were also SERS-active, the chemical and electromagnetic field enhancements, which are the two prominent mechanisms for SERS, may also play considerable roles in the excitation of the UV-absorbing DHB matrix by the visible

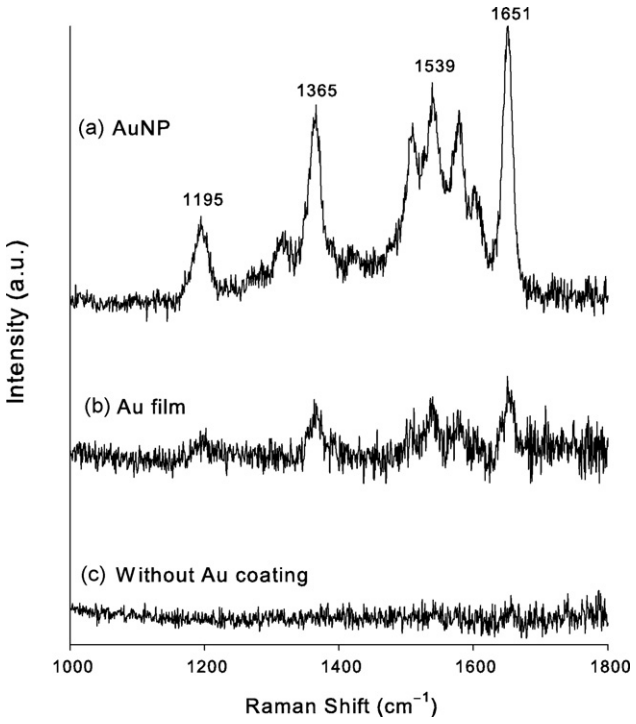

Fig. 7. The surface-enhanced Raman spectra of Rhodamine 6G obtained from the samples (a) with Au nanoparticles formed by laser ablation, (b) with un-ablated Au coating, (c) without Au coating.

laser. For example, as the gold nanoparticles couple the photon to surface plasmon efficiently, the induced electromagnetic field enhancement could promote the non-linear optical processes for the multiple photon excitation and photo-ionization of the matrix molecules. The chemical enhancement, of which the optical absorption band was broadened or red-shifted due to the interaction between absorbate molecules and the conduction electrons on the metal surface, also allows the excitation of matrix molecules by the visible laser. Besides nanoparticles, the inhomogeneous Au film remnants, which were in the form of nanostructure left on the ablated crater, could also contribute to the similar assistance effects.

4. Conclusion

We had demonstrated the visible laser MALDI using a frequency-doubled Nd:YAG laser (532 nm wavelength), by coating the UV-absorbing matrix with Au thin film, followed by laser ablation on the sample surface. The first few initial laser shots almost completely ablated bulk Au thin film on the laser spot, and the subsequent laser shots result in the observation of analyte and matrix-related ion signal that is similar to UV-MALDI from the ablated crater. The close-up inspection on the ablated region showed the formation of gold nanoparticles with size ranging from <10 nm to ~50 nm. These Au nanoparticles have high optical absorption to the visible light due to the surface plasmon resonance. Measurement with thermometer molecules showed that the heating effect, although also present with the visible laser excitation, is not as high as that of IR laser (1064 nm). The observed matrix radical ions also suggested that the ionization route for the matrix molecules is via the photo-excitation and/or photo-ionization by the visible laser, which is possible due to the electromagnetic field and the chemical enhancement effects in the vicinity of the gold nanoparticles and/or nanostructure left on the ablated crater. Gold nanoparticles or nanostructure-assisted visible laser MALDI may find application in selective ionization, in which only the analytes that are bound to the nanoparticles are ionized by the visible laser.

Acknowledgments

This work is supported by the Special Coordination Funds for Promoting Science and Technology from the Ministry of Education, Science, Sport and Culture, Japan, and the Development of System and Technology for Advanced Measurement and Analysis program (SENTAN) from Japan Science and Technology Agency (JST). L.C. Chen gratefully acknowledges the financial support from the Japan Society for the Promotion of Science (JSPS).

References

[1] D.J. Maxwell, J.R. Taylor, S. Nie, J. Am. Chem. Soc. 124 (2002) 9606–9612.
[2] Y.C. Cao, R. Jin, C.A. Mirkin, Science 297 (2002) 1536–1540.
[3] I.H. El-Sayed, X. Huang, M.A. El-Sayed, Cancer Lett. 239 (2006) 129–135.
[4] R.H. Ritchie, Surf. Sci. 34 (1973) 1–19.
[5] S. Link, M.A. El-Sayed, Int. Rev. Phys. Chem. 19 (2000) 409–453.
[6] M. Moskovits, Rev. Mod. Phys. 57 (1985) 783–826.
[7] R. Antoine, P.F. Brevet, H.H. Girault, P.F. Brevet, D. Bethell, D.J. Schiffrin, Chem. Commun. (1997) 1901.
[8] R. Antoine, M. Pellarin, B. Palpant, M. Broyer, B. Prével, P. Galletto, P.F. Brevet, H.H. Girault, J. Appl. Phys. 84 (1998) 4532–4536.
[9] M. Danckwerts, L. Novotny, Phys. Rev. Lett. 98 (2007) 026104.
[10] K. Arya, R. Zeyher, Phys. Rev. B 24 (1981) 1852–1865.
[11] A. Campion, J.E. Ivanecky III, C.M. Child, M. Foster, J. Am. Chem. Soc. 117 (1995) 11807–11808.
[12] S. Lecomte, P. Matejka, M.H. Baron, Langmuir 14 (1998) 4373–4377.
[13] K. Tanaka, H. Waki, Y. Ido, S. Akita, Y. Yoshida, T. Yoshida, T. Matsuo, Rapid Commun. Mass Spectrom. 2 (1988) 151–153.
[14] M. Karas, F. Hillenkamp, Anal. Chem. 60 (1988) 2299–2301.
[15] H. Ehring, M. Karas, F. Hillenkamp, Org. Mass Spectrom. 27 (1992) 472–480.
[16] R. Zenobi, R. Knochenmuss, Mass Spectrom. Rev. 17 (1998) 337–366.
[17] D.S. Cornett, M.A. Duncan, I.J. Amster, Anal. Chem. 65 (1993) 2608–2613.
[18] C.J. Smith, S.Y. Chang, E.S. Yeung, J. Mass Spectrom. 30 (1995) 1765–1767.
[19] L.C. Chen, D. Asakawa, H. Hori, K. Hiraoka, Rapid Commun. Mass Spectrom. 21 (2007) 4129–4134.
[20] M. Schulrenberg, K. Dreisewerd, F. Hillenkamp, Anal. Chem. 71 (1999) 221–229.
[21] J. Sunner, E. Dratz, Y.-C. Chen, Anal. Chem. 67 (1995) 4335–4342.
[22] J.A. McLean, K.A. Stumpo, D.H. Russell, J. Am. Chem. Soc. 127 (2005) 5304–5305.
[23] L.C. Chen, J. Yonehama, T. Ueda, H. Hori, K. Hiraoka, J. Mass Spectrom. 42 (2007) 346–353.
[24] L.C. Chen, T. Ueda, M. Sagisaka, H. Hori, K. Hiraoka, J. Phys. Chem. C 111 (2007) 2409–2415.
[25] M.A. Hayat, Colloidal Gold: Principles, Methods, and Applications, Academic Press, Inc., New York, 1989.
[26] M.J. Shea, R.N. Compton, Phys. Rev. B 47 (1993) 9967–9970.
[27] J. Neddersen, G. Chumanov, T.M. Cotton, Appl. Spectrosc. 47 (1993) 1959–1964.
[28] A. Delcorte, N. Medard, P. Bertrand, Anal. Chem. 74 (2002) 4955–4968.
[29] G. McCombie, R. Knochenmuss, J. Am. Soc. Mass Spectrom. 17 (2006) 737–745.
[30] J. Naban-Maillet, D. Lesage, A. Bossée, Y. Gimbert, J. Sztáray, K. Vékey, J.-C. Tabet, J. Mass. Spectrom. 40 (2005) 1–8.
[31] G. Luo, I. Marginean, A. Vertes, Anal. Chem. 74 (2002) 6185–6190.
[32] V. Karbach, R. Knochenmuss, Rapid Commun. Mass Spectrom. 12 (1998) 968–974.